Galactic Pal-eontology:
Abundance Analysis of the Disrupting Globular Cluster Palomar 5

Andreas Koch[1], and Patrick Côté[2]

[1] Department of Physics, Lancaster University, Lancaster LA1 4YB, United Kingdom
[2] National Research Council of Canada, Herzberg Astronomy and Astrophysics Program, 5071 West Saanich Road, Victoria, BC V9E 2E7, Canada

ABSTRACT

We present a chemical abundance analysis of the tidally disrupted globular cluster (globular cluster) Palomar 5. By co-adding high-resolution spectra of 15 member stars from the cluster's main body, taken at low-signal-to-noise with the Keck/HIRES spectrograph, we were able to measure integrated abundance ratios of 24 species of 20 elements including all major nucleosynthetic channels (namely the light element Na; α-elements Mg, Si, Ca, Ti; Fe-peak and heavy elements Sc, V, Cr, Mn, Co, Ni, Cu, Zn; and the neutron-capture elements Y, Zr, Ba, La, Nd, Sm, Eu). The mean metallicity of $-1.47 \pm 0.02 \pm 0.06$ dex (statistical and systematic errors) agrees well with the values from individual, low-resolution measurements of individual stars, but it is lower than previous high-resolution results of a small number of stars in the literature. Comparison with Galactic halo stars and other disrupted and unperturbed globular clusters renders Pal 5 a typical representative of the Milky Way halo population, as has been noted before, emphasizing that the early chemical evolution of such clusters is decoupled from their later dynamical history. We also performed a test as to the detectability of light element variations in this co-added abundance analysis technique and find that this approach is not sensitive even in the presence of a broad range in sodium of ~0.6 dex, a value typically found in the old halo globular clusters. Thus, while methods of determining the global abundance patterns of such objects are well suited to study their overall enrichment histories, chemical distinctions of their multiple stellar populations is still best obtained from measurements of individual stars.

Key words. Techniques: spectroscopic — Stars: abundances – Galaxy: abundances – Galaxy: evolution – Galaxy: halo – globular clusters: individual: Palomar 5

1. Introduction

Globular clusters are amongst the oldest objects in the Universe and offer unique testbeds to probe internal evolutionary processes at those early times, as well as the build-up of the Galactic halo. As to the first point, it is now well-established that any globular cluster observed to date hosts several stellar populations distinct in age, their light-element abundances (Piotto/Milone; Gratton et al. 2012, and references therein), and in a few cases in some heavy elements (e.g., Marino et al. 2015; Roederer et al. 2016). This points to proton-capture reactions acting in the hot interiors of stars associated with the first generations to have formed within the clusters. Even in observations with low-number statistics that do not allow for a representative sampling of the omnipresent Na-O anti-correlation (Carretta et al. 2009) abundance anomalies can be found, such as spreads in heavy elements that again point towards the presence of multiple stellar populations and complex enrichment histories (e.g., Koch & McWilliam 2014; Hanke et al. 2016).

Secondly, comparisons of the global chemical element abundances of globular clusters with those of the stellar Galactic halo have implications for the accretion history of the Milky Way. In this regard, several candidates have been chemically and kinematically identified as having originated in the disrupted Sagittarius dwarf galaxy (e.g., Law & Majewski 2010; Sbordone et al. 2015). Moreover, by studying light-element (in particular CN and CH) variations in globular cluster and halo stars, the fraction of the halo that was donated by disrupted satellites can be efficiently constrained (e.g., Martell & Grebel 2010)

Palomar 5 (hereafter Pal 5) is one of the most prominent examples of a stellar system in severe tidal disruption, having lost up to 90% of its mass into tidal tails that stretch over 10° over the sky (Odenkirchen et al. 2002, 2003). Previous photometric (e.g., Sandage & Hartwick 1977; Dotter et al. 2011) and low-resolution spectroscopic studies have identified it as a moderately metal-poor ([Fe/H]~ −1.4 dex) system (Smith 1985; Kuzma et al. 2015; Ishigaki et al. 2015). The latter two studies extended their analysis over broad parts of the tidal streams and they recovered a strong radial velocity gradient that is in line with simulations of the tidal disruption and can serve as input to improving halo mass models (Dehnen et al. 2004; Odenkirchen et al. 2009; Pearson et al. 2015). However, no metallicity gradient across the tails has been found. Smith et al. (2002) performed the first and only measurements of four stars at intermediate spectral resolution and high Signal-to-Noise ratio (SNR), suggesting that Pal 5 resembles the Galactic halo and higher-mass globular clusters in many regards; one exception was a lower-than-average [α/Fe] abundance ratio, which, at ~0.16 dex, was found to lie significantly below the plateau value of ~0.4 dex inhabited by globular cluster and field stars at similar metallicities. Furthermore, Smith (1985) and Smith et al. (2002) detected large abundance variations in the light elements (C, N, Na and Al) and concluded that whatever evolutionary processes are responsible for those variations are oblivious to the globular cluster's present-day mass and that they were already imprinted at early times when the cluster still retained their initial mass.

Many remote Milky Way globular clusters are faint systems, which leads to time-expensive observation strategies; thus one path to obtaining detailed chemical abundance information is to use integrated light spectroscopy (e.g., McWilliam & Bernstein 2008) or to co-add individual spectra at low SNR to emulate a higher-quality spectrum of a known underlying stellar population (Koch et al. 2009; Koch & Côté 2010). Following our work on the outer halo clusters Pal 3 and Pal 4 we now turn to the closer (R$_\odot$=23 kpc) object Pal 5.

In §2 we describe our target list and observations, followed by a discussion of the radial velocity measurements and cluster membership assessments in §3. Details on the co-added abundance determination and error analysis are given in §4 and we present the results in §5, with a focus on comparison with other globular clusters in §6. In §7 we briefly comment on the detectability of abundance variations with our approach, before concluding in §8.

2. Targets and observations

The Pal 5 data discussed here were taken as part of a broader program to study the internal dynamics of outer halo globular clusters (see, e.g., Côté et al. 2002, Jordi et al. 2009, Baumgardt et al. 2009; Frank et al. 2012). Our Pal 5 target stars were chosen from the red giant branch (RGB) and asymptotic giant branch (AGB) sequences identified in the early photometric studies of Sandage & Hartwick (1977; SH77) and the unpublished photometry and astrometry from Cudworth, Schweitzer and Majewski (CSM; see Schweitzer et al. 1993). Our target stars reach out to ~2 half-light radii and all lie well within the cluster's tidal radius, avoiding the cluster's tidal features (Odenkirchen et al. 2003). Of course, the concept of tidal radius for such a highly disturbed object is largely meaningless and we refrain from investigating possible spatial trends in kinematics or abundance. Properties of the target stars and HIRES observations are given in Table 1. In Fig. 1, we show their location in a color-magnitude diagram (CMD) based on photometry from the Sloan Digital Sky Survey (SDSS; Alam et al. 2015).

Table 1. Log of target stars

Star[a]	α (J2000.0)	δ (J2000.0)	Exp. time [s]	S/N[b] [pixel^{-1}]
CSM-003	15 16 15.93	−00 09 28.79	180	6
CSM-029	15 16 13.99	−00 09 33.39	300	7
CSM-030	15 16 16.37	−00 10 29.76	300	6
CSM-032	15 16 09.52	−00 02 39.64	240	7
CSM-045	15 16 20.85	−00 08 42.72	180	9
CSM-174	15 16 07.67	−00 10 18.64	180	7
CSM-598	15 16 19.18	−00 11 31.11	600	8
SH77-E	15 15 58.83	−00 05 17.02	180	10
SH77-F	15 15 56.05	−00 06 05.67	180	12
SH77-G	15 16 08.61	−00 08 03.19	180	8
SH77-H	15 15 52.54	−00 07 40.47	180	7
SH77-J	15 15 49.64	−00 07 00.73	240	7
SH77-K	15 16 06.47	−00 07 00.91	240	7
SH77-L	15 16 01.95	−00 08 02.75	240	8
SH77-M	15 15 46.08	−00 09 08.42	240	6
SH77-N	15 15 59.45	−00 08 59.69	240	6
SH77-14	15 16 08.26	−00 07 38.01	600	7
SH77-U	15 15 54.73	−00 06 54.95	300	5

Notes. [a] Star-IDs from SH77 and CSM. [b] Given at 6600 Å.
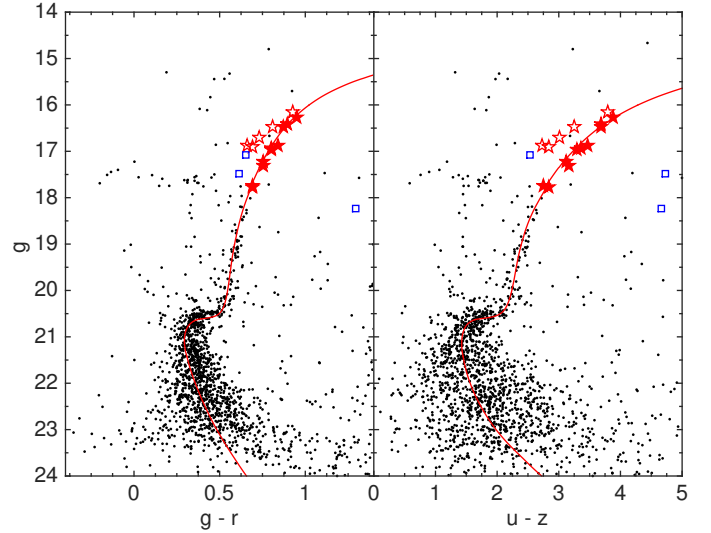
Fig. 1. CMD using SDSS photometry of stars within two half-light radii. Blue squares indicate foreground stars, open red symbols are AGB candidates, while our RGB targets are shown as solid stars. Dartmouth isochrones indicative of the globular cluster's parameters.

3. Radial velocities and membership

Our observations were taken on May 31, 1998 using the HIRES echelle spectrograph (Vogt et al. 1994) on the Keck I telescope with the C1 decker (slit width of 0.86″) and 1×2 binning, which provides a spectral resolution of R=45 000. The data were reduced with the Makee[1] pipeline. The radial velocity of each star was measured by cross-correlating its spectrum against that of a master template created during each run (see below) from observations of IAU standard stars. In order to minimize possible systematic effects, a master template for each observing run was derived from an identical subsample of IAU standard stars. From each cross-correlation function, we measured both v_{HC}, the heliocentric radial velocity, and R_{TD}, the Tonry & Davis (1979) estimator of the strength of the cross-correlation peak.

During our broader Keck program, which spanned seven observing runs in 1998 and 1999 (13 nights in total), we obtained 53 distinct radial velocity measurements for 23 different RGB and subgiant stars belonging to Pal 3, Pal 4, Pal 5, Pal 14, NGC 7492 and NGC 2419. Using these repeat measurements and following the procedures described in Vogt et al. (1995), we derived an empirical relationship between our radial velocity uncertainties, $\epsilon(v_{HC})$, and the strength of cross correlation peak: $\epsilon(v_{HC}) = \alpha/(1 + R_{TD})$, where $\alpha = 9.0^{+2.4}_{-1.6}$ km/sec (90% confidence limits). The final radial velocities and their uncertainties are recorded in Table 2.

Several spectroscopic studies have since been carried out for Pal 5. All of the four stars analysed by Smith et al. (2002), using Keck/HIRES at high SNR but lower resolution than ours, are included in our data set as well, whereas none of the stars are included in Odenkirchen's et al. (2009) kinematic study. Odenkirchen et al. (2002) performed a kinematic study on their ESO/UVES spectra with high-resolution, but lowSNR (~10 pixel^{-1}), of which ten stars are also in our present sample. We observed eleven stars in common with the work of Kuzma et

---

[1] MAKEE was developed by T. A. Barlow specifically for reduction of Keck HIRES data. It is freely available on the World Wide Web at the Keck Observatory home page, http://www2.keck.hawaii.edu/inst/hires/makeewww

Table 2. Properties of the target stars

Star	u	g	r	i	z	v_{HC} [km s^{-1}]	Type[a]	T_{eff} [K]	$\log g$	ξ [km s^{-1}]	[Fe/H]$_{MgT}$
CSM-003	18.934	16.869	16.027	15.673	15.461	-52.19 ± 0.50	RGB	4473	1.40	1.51	-1.32
CSM-029	19.205	17.296	16.538	16.217	16.033	-57.42 ± 0.54	RGB	4607	1.67	1.55	-1.33
CSM-045	18.564	16.279	15.327	14.921	14.679	-59.28 ± 0.37	RGB	4317	1.03	1.80	-1.45
SH77-F	18.622	16.419	15.524	15.157	14.933	-58.51 ± 0.40	RGB	4410	1.16	1.38	-1.43
SH77-G	18.681	16.464	15.592	15.217	15.000	-58.28 ± 0.45	RGB	4418	1.19	1.12	-1.42
SH77-K	18.950	16.926	16.125	15.783	15.597	-59.25 ± 0.46	RGB	4531	1.46	1.32	-1.33
SH77-L	18.905	16.955	16.155	15.816	15.616	-58.90 ± 0.47	RGB	4536	1.48	1.34	-1.38
SH77-N	19.057	17.210	16.453	16.128	15.943	-60.32 ± 0.59	RGB	4601	1.63	1.30	-1.33
SH77-14	19.437	17.772	17.082	16.787	16.601	-58.41 ± 0.53	RGB	4731	1.94	1.61	-1.32
SH77-U	19.329	17.735	17.040	16.744	16.578	-59.09 ± 0.90	RGB	4722	1.92	1.02	-1.13
CSM-032	18.585	16.894	16.201	15.911	15.749	-59.00 ± 0.58	AGB	4737	1.47	1.46	-1.44
CSM-174	18.410	16.481	15.676	15.344	15.161	-61.14 ± 0.50	AGB	4545	1.17	1.16	-1.49
SH77-E	18.393	16.142	15.219	14.830	14.601	-57.48 ± 0.38	AGB	4358	0.88	1.41	-1.46
SH77-H	18.514	16.690	15.961	15.648	15.493	-57.24 ± 0.58	AGB	4653	1.33	1.75	-1.37
SH77-J	18.466	16.863	16.203	15.911	15.744	-57.38 ± 0.62	AGB	4773	1.48	0.12	-1.58
CSM-030	21.280	17.481	16.865	16.533	16.558	-38.32 ± 0.57	FG	…	…	…	…
CSM-598	20.772	18.226	16.932	16.409	16.104	-14.33 ± 0.61	FG	…	…	…	…
SH77-M	18.500	17.079	16.426	16.131	15.959	20.18 ± 1.11	FG	…	…	…	…

Notes. [a] Stellar type based on CMD and spectral properties: red giant branch (RGB), asymptotic giant branch (RGB), or foreground (FG) dwarf.

al. (2015), who obtained velocity and calcium-triplet metallicity measurements based on low-resolution ($R \sim10000$) spectroscopy with the AAOmega multi-fibre instrument. Finally, one of our stars is also included in the data of Ishigaki et al. (2016) who used low-resolution ($R \sim7000$) spectra to gather kinematics, metallicities, and [α/Fe] ratios.

The mean heliocentric velocity of -58.3 ± 0.5 km s^{-1} we find for Pal 5 is in excellent agreement with all previous studies of the central regions to within the uncertainties. The dispersion of 1.8 ± 0.3 km s^{-1} from our data is slightly higher than the literature values of typically 1.1 ± 0.3 km s^{-1}, but this may be due to the lower number of stars we observed or to our confinement to the more central parts of the cluster.

Three of our targets turned out to be non-members based on their strongly deviating velocities. While the presence of a strong velocity gradient throughout this tidal system (e.g., Odenkirchen et al. 2002) could in principle render these stars related to Pal 5, the appearance of their spectral features such as broad, gravity-sensitive Mg triplet lines or the Ca 6162Å-line clearly indicates that they are foreground dwarfs.

As the CMD in Fig. 1 implies, five of the targets are located on the AGB, as was also suggested for four of them by Odenkirchen et al. (2002). The separation of our sample into RGB, AGB, and foreground stars is indicated in Table 2.

4. Analysis

The original aim in acquiring this data set was to study the kinematics of Galactic halo clusters (see §2) and so the exposure times were chosen to be in the range 3–10 minutes, thus operating at low (SNR; Table 1; see also Odenkirchen et al. 2002). While this SNR is adequate for measuring accurate radial velocities, a detailed chemical analysis of individual stars is precluded. Thus, we resort to our method of co-adding spectra in the manner outlined in Koch et al. (2009) and Koch & Côté (2010).

4.1. Stellar parameters

Stellar effective temperatures of the individual stars were obtained from their (V−I) colors using the calibrations of Ramírez

& Meléndez (2005). To this end, we transformed the SDSS g, r, i magnitudes to the Johnson-Cousins system following the prescriptions of Jordi et al. (2006) and adopting a cluster reddening of E(B−V)=0.08 mag (Dotter et al. 2011). The typical uncertainty on T_{eff} due to the (small) photometric errors in the SDSS and the calibrations is ~50 K.

Next, the surface gravities were obtained using the standard equations of stellar structure, where we used the above temperature, a stellar mass of 0.8 M$_\odot$ for the RGB and 0.6 M$_\odot$ for AGB stars, and a distance to Pal 5's center of 23.2 kpc. As an initial estimate of the stars' metallicity that enters the bolometric corrections we adopted the photometric globular cluster mean of -1.35 dex. One uncertain factor is the pronounced presence of mass segregation within Pal 5 and throughout its tails (Koch et al. 2004), which could also affect the analysis of our stars that are located throughout the cluster. Propagating the errors on all the above quantities translates into typical gravity uncertainties of 0.15 dex.

Similar to our previous work (Koch et al. 2009; Koch & Côté 2010), we derived microturbulence velocities, ξ, using an empirical calibration of ξ with T_{eff} based on the halo stars of Roederer et al. (2014). The inferred uncertainty from the scatter around this relation is 0.10 km s^{-1}.

While a global cluster metallicity is available for Pal 5 (e.g., Dotter et al. 2011) and previous low-resolution studies have measured metallicities of individual stars (e.g., Kuzma et al. 2015; see also §5.1), we opted to obtain initial metallicities of our targets that enter the stellar atmospheres from from the Mg I line index. This index uses the strong Mg triplet lines at 5167 and 5173Å and is defined and calibrated on the scale of Carretta & Gratton (1997) as in Walker et al. (2007) and Eq. 2 in Koch et al. (2009). For this, we assume a horizontal branch magnitude of V$_{HB}$=17.51 mag (Harris 1996 [2010 edition]). All stellar parameters we have used in creating our stellar atmospheres are listed in Table 2 and plotted in Fig. 2.

4.2. Co-added abundance measurements

Consistent with our previous work, we have median-combined the spectra, irrespective of evolutionary status, after weighting
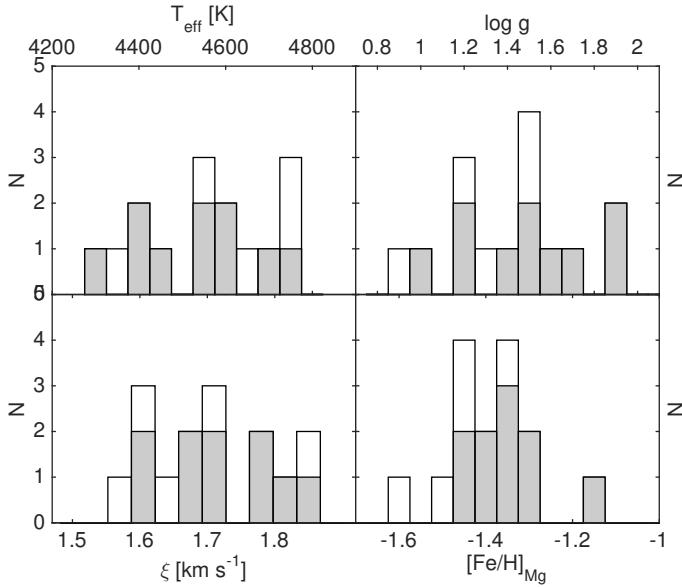
Fig. 2. Histogram of stellar parameters. Solid bars are for RGB stars and clear ones for the AGB subsample.

by their SNR. Equivalent widths (EWs) were measured from the line lists of Koch et al. (2016) and Ruchti et al. (2016) by fitting Gaussian profiles with IRAF's *splot* task. These line lists and the EW measurements are presented in Table 3.

Table 3. Linelist

λ [Å]	Species	E.P. [eV]	$\log gf$	$\langle EW \rangle$ [mÅ]
5682.633	Na I	2.102	−0.700	61.3
5688.205	Na I	2.104	−0.404	91.9
6154.225	Na I	2.102	−1.547	11.8
6160.747	Na I	2.104	−1.246	31.0
4571.096	Mg I	0.000	−5.623	149.6
4702.991	Mg I	4.346	−0.440	171.5
5711.088	Mg I	4.346	−1.724	76.62

Notes. Table 3 is available in its entirety in electronic form via the CDS.

In the following analysis, we have used the 2014 version of the stellar abundance code MOOG (Sneden 1973). From the stellar parameters derived in §4, we created individual stellar atmospheres for each star. Specifically, the ATLAS grid of Kurucz' one-dimensional 72-layer, plane-parallel, line-blanketed models without convective overshoot was interpolated assuming local thermodynamic equilibrium (LTE) for all species, together with the α-enhanced opacity distribution functions, AODFNEW. We then computed theoretical EWs for all transitions using MOOG's *ewfind* driver and combined them into a mean $\langle EW \rangle$ by applying the same SNR-based weights as for the observed spectra (see, e.g., Eq. 1. in Koch & Côté 2010). Finally, the abundance ratio of each element was varied until the co-added $\langle EW \rangle$ matched the observed EW for each line to yield an integrated abundance ratio.

4.3. Abundance errors

We quantified the measurement error by standard procedures: firstly, the statistical error is given by the 1σ line-to-line scatter and the number of lines, N, used to measure an element's abun-

dance, each of which are listed in Table 4. For a few elements, only one weak feature was measurable and we varied the observed EW by 5 mÅ for those cases (which yielded reasonable fits to the line profile in *splot*). This led to typical uncertainties in the respective abundances of 0.15 dex.

Secondly, to determine the systematic uncertainties, we varied each of the stellar parameters by their typical uncertainty ($T_{eff} \pm 50$ K; $\log g \pm 0.15$ dex; $\xi \pm 0.10$ km s^{-1}) and re-ran the co-addition scheme. Note that this presupposes that all of the stars are affected by the same amount of error and the same sense of departure from the un-altered values. The difference for each element upon this variation in each parameter is listed in Table 4; there, we also indicate the effect of switching from the α-enhanced opacity distribution functions to the solar-scaled distributions, ODFNEW. Due to the strong correlations between temperature, gravity, and, as per our construction, the microturbulence, also the systematic uncertainties are not independent of each other. Thus, we caution that the total error we list in Table 4, which is merely the quadratic sum of all contributions, should be taken as a conservative upper limit at most.

In Koch & Côté (2010), we investigated further error sources such as radial velocity uncertainties which can lead to additional line broadening, but found that this accounts for less than 0.04 dex in the error budget. Likewise, the accidental inclusion of foreground stars would add no more than 0.02 dex of abundance uncertainty.

5. Abundance results

The results from our co-added abundance measurements are presented in Table 3. All our abundances are on the scale of solar abundances from Asplund et al. (2009). Figures 3–5 show these abundance ratios in comparison with other Galactic components, such as halo field stars (from Roederer et al. 2014), the bulge (Johnson et al. 2012, 2014), and the disks (Koch & Edvardsson 2002; Bensby et al. 2014). Furthermore we added globular cluster data for M5 as a representative of an undisturbed system at comparable metallicity (Ivans et al. 2001), the outer halo globular clusters Pal 3 and Pal 4 (Koch et al. 2009; Koch & Côté 2010), and several objects that have been associated with the disrupting Sgr dwarf galaxy (see the caption of Fig. 3 for the color coding): Pal 12 (Cohen 2004); Terzan 7 (Sbordone et al. 2005); Arp 2 (Mottini et al. 2008); Terzan 8 and the massive M 54 (Carretta et al. 2014), and NGC 5053 and 5634 (Sbordone et al 2015). Finally, the tidally disturbed cluster NGC 5466 (Lamb et al. 2015) is shown as an orange hexagon.

5.1. Iron abundance and metallicity

The ensuing metallicity distribution from the Mg index (Fig. 2, bottom left) indicates a mean metallicity of −1.38 dex. This is in excellent agreement with both photometric values of −1.4 dex (Dotter et al. 2011) and, to within their (large) uncertainties, the low-resolution mean values of Kuzma et al. (2015) and Ishigaki et al. (2016) of −1.48 ± 0.10 and −1.35 ± 0.06, respectively. All values can be reconciled if we split our sample into RGB stars only (−1.33 ± 0.09 dex) versus an AGB-only subset (−1.47 ± 0.08 dex). Smith et al. (2002) found a more metal-rich mean value, −1.28±0.03 dex, from four high-SNR, medium resolution spectra.

From the co-added spectrum, we measured 89 Fe I and 13 Fe II lines to arrive at an Fe-abundance that agrees well with all aforementioned values, namely [Fe/H]=−1.47 ± 0.02 ± 0.06 dex

Table 4. Abundance results from co-added spectra. Abundance ratios for ionized species are given relative to Fe II. For iron itself, [Fe/H] is listed. The line-to-line scatter σ and number of measured lines, N, determine the statistical error, while the systematic uncertainties are indicated in the last five columns.

Species	[X/Fe]	σ	N	$\Delta T_{eff}\pm50$ K	$\Delta \log g\pm0.15$ dex	$\Delta\xi\pm0.1$ km s^{-1}	ODF	σ_{sys}
Fe I	−1.47	0.18	89	±0.05	< 0.01	∓0.03	< 0.01	0.06
Fe II	−1.39	0.24	12	∓0.06	±0.10	∓0.02	−0.05	0.13
Na I	0.35	0.16	4	∓0.04	±0.01	±0.01	−0.01	0.04
Mg I	0.25	0.32	3	∓0.04	±0.01	±0.02	−0.02	0.05
Si I	0.32	0.25	9	<0.01	∓0.02	<0.01	−0.01	0.02
Ca I	0.35	0.25	21	∓0.06	±0.01	±0.05	−0.04	0.09
Sc I	0.16	0.07	2	∓0.09	±0.01	<0.01	<0.01	0.09
Sc II	0.03	0.13	6	±0.01	∓0.06	±0.02	−0.02	0.07
Ti I	0.10	0.22	22	∓0.09	±0.01	±0.03	−0.03	0.10
Ti II	0.10	0.29	10	±0.01	∓0.06	±0.06	−0.06	0.10
V I	−0.10	0.21	9	∓0.09	±0.01	±0.01	−0.01	0.09
Cr I	−0.27	0.33	5	∓0.09	±0.01	±0.03	−0.03	0.10
Cr II	0.04	…	1	±0.03	∓0.06	±0.02	−0.02	0.07
Mn I	−0.24	0.23	8	∓0.06	±0.01	±0.02	−0.02	0.06
Co I	−0.21	0.08	3	∓0.05	<0.01	±0.01	−0.01	0.05
Ni I	−0.07	0.24	18	∓0.03	∓0.01	±0.01	−0.02	0.04
Cu I	−0.58	0.22	2	∓0.06	∓0.01	±0.03	−0.03	0.07
Zn I	−0.04	0.05	2	±0.02	∓0.04	±0.03	−0.03	0.06
Y II	−0.27	0.40	5	∓0.02	∓0.05	±0.06	−0.07	0.11
Zr II	−0.19	0.19	2	<0.01	∓0.06	±0.01	−0.02	0.06
Ba II	0.34	0.16	5	∓0.02	∓0.04	±0.06	−0.09	0.12
La II	0.07	…	1	∓0.01	∓0.06	±0.01	−0.01	0.06
Nd II	0.33	…	1	∓0.01	∓0.06	±0.02	−0.02	0.07
Sm II	0.18	0.09	4	∓0.01	∓0.06	±0.01	−0.01	0.06
Eu II	0.48	…	1	<0.01	∓0.06	<0.01	−0.01	0.06

(statistical and systematic errors, respectively) based on the neutral species. Ionization equilibrium is marginally reached in this co-added approach, at [Fe I/Fe II]=−0.08 ± 0.07 dex (Table 3). In the following discussions, abundance ratios of ionized species will be referenced to the iron abundance from Fe II lines.

None of the low-resolution spectroscopic studies introduced above suggested any signs of a metallicity gradient across the tidal tails or the face of the cluster. However, since the second stellar populations, usually slightly more metal rich, usually form in the denser central regions of the globular cluster (e.g., D'Ercole et al. 2008) and given that tidal stripping gradually removes the outer portions of stellar systems (e.g., Koch et al. 2004), such metallicity gradients would be expected in the presence of distinct multiple populations. Our stars are located between 0.8′ and 5.8′ (0.3–2.1 half-light radii) from the cluster center. Here, we note a metallicity "gradient" in the sample from the Mg index of ~0.15 dex over the extent of the data, although we caution that this should be considered marginal due to the large uncertainties in the index measurements. All other studies rather agree on a low scatter in the metallicities of Pal 5 across its main body.

5.2. Light elements: Na

Unfortunately, both of the strong Na D lines fall on the gap between adjacent orders so we derived the Na-abundance from the weaker 5682, 5688, 6154, and 6160 Å lines. No oxygen lines were detectable in the co-added spectrum. At 0.35 dex, the mean, co-added [Na/Fe] abundance ratio of Pal 5 is high compared to halo stars at the same metallicity, which usually show solar to subsolar values. The corrections for NLTE in individual stars with stellar parameters as in our Pal 5 sample are on the order of −0.10 dex (Lind et al. 2011). Generally, the presence of strong Na lines could provide evidence of Na-strong, second generation

globular cluster stars amongst the sample. In fact, a pronounced light-element spread in Pal 5 of 0.3 dex (with a full range of 0.6 dex) was already noted by Smith et al. (2002). We further discuss the sensitivity of our analysis method to these light element variations in §6.

5.3. Alpha-elements: Mg, Si, Ca, Ti

Pal 5 shows a mild enhancement in the α-elements, which overlaps with the halo distribution by merit of the latter's broad scatter. A straight average over all four elements Mg,Si,Ca, and Ti yields [α/Fe]=0.26 dex, although differences in each element's production channel renders other weighting schemes more appropriate. Smith et al. (2002) found the abundances of these elements to be significantly lower (<[Si,Ca,Ti/Fe]>=0.16, while we find 0.26 from those three elements) when compared to halo field stars or the similarly metal-poor globular cluster M 5 (Ivans et al. 2001; Koch & McWilliam 2010). Our data indicate a depletion from the α-plateau that is most pronounced in Mg in Ti, which both still overlap with the M 5-abundances (cyan triangles in Figs. 4–6) to within the errors. Our values are furthermore fully consistent with the measurements of individual stars in the M 54, which, at −1.5 has a very similar metallicity to Pal 5. This massive globular cluster is thought to be the central cluster of the Sgr dwarf galaxy. Finally, we note that there is an excellent ionization balance between Ti I and II when taken relative to Fe I and Fe II.

5.4. Fe-peak and heavy elements: Sc, V, Cr, Mn, Co, Ni, Cu, Zn

None of the Fe-peak elements show a surprise as they all fall in the regime of the halo field star and globular cluster distributions (Fig. 4). We note that ionization equilibrium is not fulfilled for
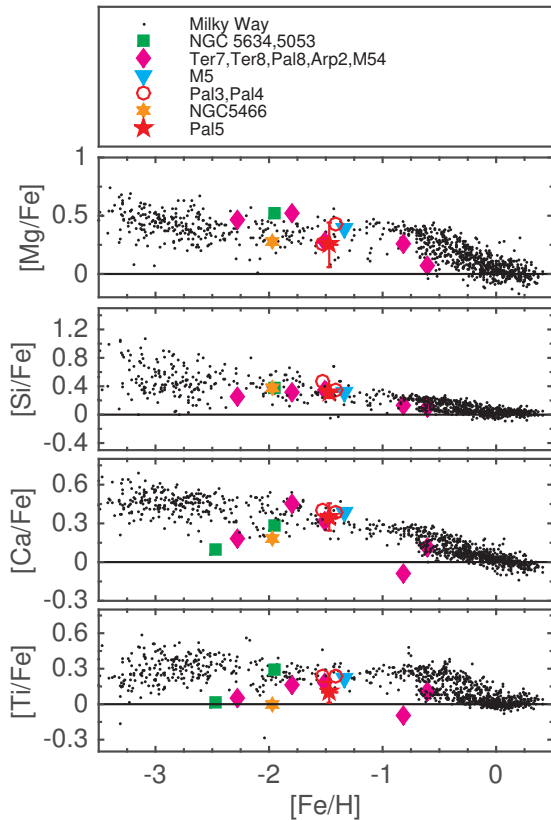
Fig. 3. Abundance results for the α-elements. Literature data for the Milky Way (black dots) are from: halo – Roederer et al. (2014); bulge – Johnson et al. (2012,2014); disks – Bensby et al. (2014). Pal 5 is shown as a red star symbol, while other globular clusters are from Sbordone et al. (2015) – NGC 5053, 5634 (green squares); Cohen (2004); Sbordone et al. (2007); Mottini et al. (2008); Carretta et al. (2014) for Pal 12, Ter 7, Arp 2, Ter 8, and M 54 (magenta diamonds). M 5 is shown as a cyan triangle (Ivans et al. 2001), the outer halo globular clusters Pal 3 and Pal 4 as open circles (Koch et al. 2009; Koch & Côté 2010), and the disrupted NGC 5466 as orange hexagon (Lamb et al. 2015).

Sc and Cr, but the measurements of their minority species are usually based on only one or two lines.

5.5. Neutron-capture elements: Zr, Y, Ba, La, Nd, Sm, Eu

All of these elements have sound measurements, while [Eu/Fe] is based on a marginal detection (EW=17 mÅ) of the 6645 Å line. As for the remainder of the elements, also the neutron-capture elements we determined (Fig. 5) are fully compatible with Galactic halo stars and globular clusters at similar metallicities. This indicates that Pal 5's early evolution was governed by the same enrichment processes as other, old and metal-poor globular clusters over a broad range of masses so that the subsequent strong mass-loss had no bearing on the chemical abundance patterns observed today.

6. Comparison with other clusters

The distinguishing feature of Pal 5 is clearly its severe state of tidal disruption. Nevertheless, all chemical abundance information had already been imprinted on its stars at an early stage before this dynamical alteration began. Thus, chemically speaking,
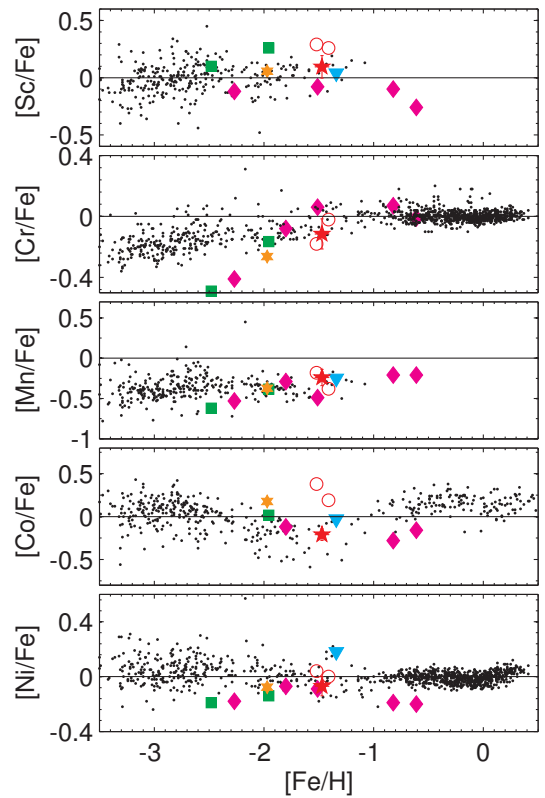

Fig. 4. Same as Fig. 3, but for Fe-peak and heavy elements.

it is a typical representative of the old, metal-poor halo population. This is highlighted in Figs. 3–5 through a comparison to a selection of other globular clusters that are interesting for a variety of reasons.

M5 is an inner halo (R_{GC}=6 kpc) globular cluster with a metallicity similar to that of Pal 5. It is presently much more massive than the very low-mass Pal 5 (at $M_V = -8.81$ vs. -5.17 mag) and shows only mild evidence of tidal distortion (Jordi & Grebel 2010). While Smith et al. (2002) note a lower [α/Fe] ratio in Pal 5 compared to M5, all other elements measured in that study and by us are fully compatible with those in M5.

In Figs. 3–5 we overplotted several objects that have been associated with Sagittarius. Given the complex star formation and enrichment history of this massive Galactic satellite, those globular clusters span a broad range of metallicities from ∼ −0.5 to below −2 dex. In this regard, younger outer halo clusters such as Pal 12 ([Fe/]H=−0.8 dex; R_{GC}=16 kpc) show the depleted [α/Fe] ratios typical of environments with a low star formation efficiency. This value amounts to 0.06 dex for Pal 12 (Cohen 2014) and is significantly lower than found in Pal 5, despite the latter already having an enhancement lower than the halo average. Other such clusters, such as M 54 at the same metallicity as Pal 5, are very similar in most of the elements, again indicating that the dynamical history of these systems has not affected any of their basic chemical properties.

Located beyond 90 kpc, Pal 3 and Pal 4 are amongst the the most globular clusters in the Milky Way halo. Despite their younger ages (∼10 Gyr compared to 12 Gyr for other, typical old globular clusters), the main conclusion from the co-added abundance analyses of Koch et al. (2009) and Koch & Côté (2010) was that these outer halo clusters are chemically indistinguishable from the older ones in the inner halo and have thus experi-
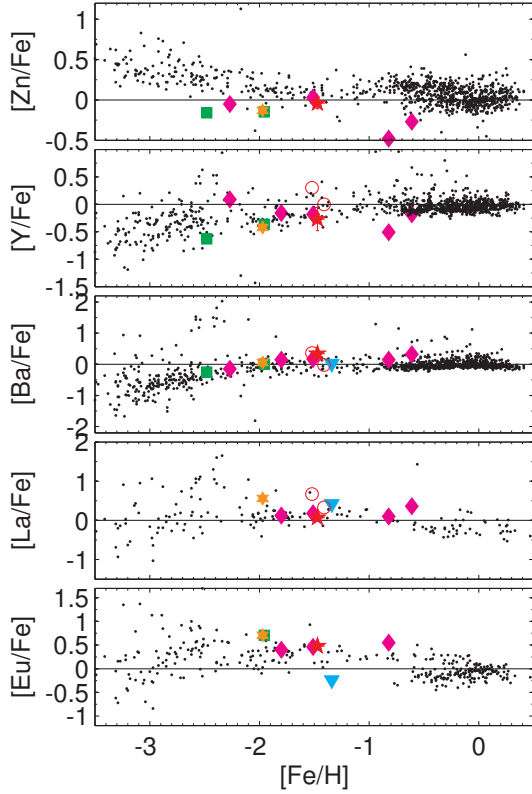
Fig. 5. Same as Fig. 3, but for neutron-capture elements. Eu disk abundances are from Koch & Edvardsson (2002).

enced similar enrichment histories. Pal 3 and 4 have metallicities comparable to that of Pal 5 and most of their chemical abundances are very similar. In particular, Pal 3 has a lower mean [Mg/Fe] ratio that is identical to the one we found for Pal 5. In a few cases, other element ratios deviate from the halo distribution and from Pal 5's abundances, such as higher Sc and enhanced Co for both clusters, and elevated Zn and La abundances in Pal 3; for the remaining elements, all the Pal's element ratios agree within the uncertainties. Finally, we note that both of the studies mentioned above used the same technique of co-adding spectra and yielded very similar abundance results and precisions.

NGC 5466 is metal-poor ([Fe/H]=−1.97 dex) and shows tidal tails extending ∼ 4° (Belokurov et al. 2006). An optical and infrared abundance analysis by Lamb et al. (2015) revealed typical globular cluster abundance patterns for all studied elements in that it shows light element variations and neutron-capture abundances indicative of pollution from AGB stars. Despite its state of distrubance, and a possible connection to the Sgr dwarf galaxy, Lamb et al. (2015) could not detect any obvious differences from the prevailing halo distribution at those low metallicities. NGC 5466's α-elements are depleted to a similarly extent as found for Pal 5, albeit at half a dex lower metallicity. We note that those authors used a combination of optical and infrared spectroscopy and accounted for departures from LTE for several elements so that slight differences to the literature halo and globular cluster samples (performed in LTE from optical data) occur naturally.

Another interesting reference object is the bulge cluster NGC 6712 at [Fe/H]=−1.01 dex (Yong et al. 2008). This object has lost a considerable amount of its mass as manifested in its mass- and luminosity functions (de Marchi et al. 1999). It also shows O and Na abundance variations as strong as in any other globular cluster, but are not seen in halo field stars (e.g., Geisler et al. 2007). From the sheer, large extent of the O and Na abundance variations in their sample of five stars (with full range of of 0.6 dex and 1σ scatter of 0.28 dex both in Na and O), Yong et al. (2008) concluded that this globular cluster must have been much more massive in the past in order to allow for these element variations to develop across the cluster's multiple populations. Such large spreads were also found by Smith et al. (2002) in Pal 5 , which also has lost up to 90% of its initial mass. Therefore, it is timely to ask whether such light element variations could be detected in an abundance analysis based on co-added spectra.

7. Light element variations

The wavelength range of our spectra allowed us, in principle, to estimate the carbon-richness of the stars based on the CH G-band at ∼4300 Å. The derived CH-index provides a well-calibrated tool measured on low-resolution spectra, which often results in bimodal distributions indicative of the complex chemical enrichment processes in globular clusters (e.g., Smith 1985; Kayser et al. 2008). While we could attempt to measure a similar band-index, we note that our spectra cut-off redwards of the bluest end of the CH-bandpass commonly used in such population studies (i.e., at 4298 Å instead of the limit of 4285 Å; e.g., Eq. 2 in Kayser et al. 2008. This renders the zeropoint of our measurements incommensurable. It is, however, still very useful in identifying possible abundance spreads or outliers such as CH-strong or -weak stars.
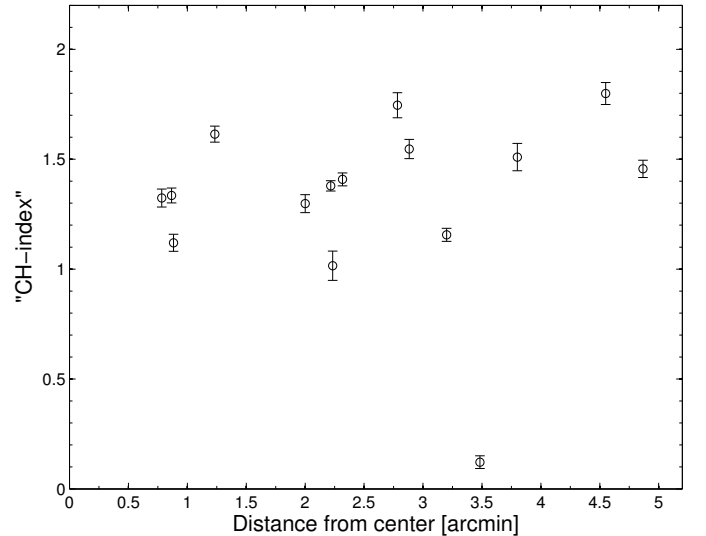
Fig. 6. Pseudo-CH-index versus position in the globular cluster. The CH-weak AGB-star Pal-J clearly stands out.

As Fig. 6 indicates, one object (the AGB-star J at 3.5′ or 1.3 half-light radii) has a significantly lower CH-index indicating that it is carbon-weak. The CH band strength is usually correlated with the N-abundance, which is commonly quantified by CN-band index, in the sense that CH-weak stars tend to be CN-strong (e.g., Kayser et al. 2008; Martell et al. 2010) so we should expect star J to also have a significantly stronger CN band. However, as already noted by Smith (1985), this is not the case and star J is also CN-weak, which prompted him to

invoke metallicity effects to explain the extraordinarily low C-abundance.

Our method explicitly assumes that there is none of the chemical elements shows any abundance spread. Given the evidence of light-element (O, Na, Mg, Al) variations in every globular cluster studied to date, this is clearly a false premise. In order to test how our co-added abundance derivation responds to the presence of an abundance spread, we emulated a Na-O anti-correlation by randomly populating this abundance space with 10^5 stars, following the dilution model for M5 from Carretta et al. (2009). This globular cluster is very similar to Pal 5 in most respects (Ivans et al. 2001; Carretta et al. 2009). The ratio of first generation (low-Na, high-O) to second generation stars (high-Na, low-O) was chosen as 30:70 (e.g., Carretta 2013). Out of this random sample, we drew 15 random values (corresponding to the number of targets) and predicted individual EWs for each with MOOG, ultimately co-adding them as before (§4.2).

As a result, we found no correlation of the combined EW with the sampling of Na-poor and Na-rich stars from the mock cluster, as quantified by the [Na/Fe] interquartile range of the input sample. This means that co-added EW measurements or syntheses of integrated-light spectra (as also in, e.g., Koch & Côté 2010; Sakari et al. 2013; Schönebeck et al. 2014) are rather insensitive to any spread in chemical elements, as exemplified here by sodium; even more so, since for Pal 5, a large Na-spread of 0.6 dex is already known from high-resolution measurements of four individual stars (Smith et al. 2002).

8. Summary and conclusions

We determined chemical abundance ratios for various tracers of chemical evolution in the tidally disrupted GC Pal 5 using the co-addition technique we developed in earlier studies of remote Milky Way satellites. While this technique only allows us to measure the integrated properties of the stellar system, our results are fully compatible with results from a low number of individual high-resolution spectra (four stars of Smith et al. 2002). As a result, we found that Pal 5 is not unusual in any regard and that it follows the abundance trends of metal-poor GCs very closely, indicating that tidal perturbations over the course of Gyrs of evolution have no impact whatsoever on the chemical properties of these systems.

We were able to measure mean abundance ratios for 20 elements to high precision, however, our statistical tests have shown that the method of co-adding spectra is not sensitive to disentangling abundance variations such as the Na-O anti-correlation, even if spreads of the typical, high degree of 0.6 dex are present. To better characterize those, individual spectra of a large number of stars are still the most viable course.

References

Alam, S., Albareti, F. D., Allende Prieto, C., et al. 2015, ApJS, 219, 12
Asplund, M., Grevesse, N., Sauval, A. J., & Scott, P. 2009, ARA&A, 47, 481
Baumgardt, H., Côté, P., Hilker, M., et al. 2009, MNRAS, 396, 2051
Belokurov, V., Evans, N. W., Irwin, M. J., Hewett, P. C., & Wilkinson, M. I. 2006, ApJ, 637, L29
Bensby, T., Feltzing, S., & Oey, M. S. 2014, A&A, 562, A71
Carretta, E., & Gratton, R. G. 1997, A&AS, 121, 95
Carretta, E., Bragaglia, A., Gratton, R. G., et al. 2009, A&A, 505, 117
Carretta, E. 2013, A&A, 557, A128
Cayrel, R., Depagne, E., Spite, M., et al. 2004, A&A, 416, 1117
Côté, P., Djorgovski, S. G., Meylan, G., Castro, S., & McCarthy, J. K. 2002, ApJ, 574, 783
Dehnen, W., Odenkirchen, M., Grebel, E. K., & Rix, H.-W. 2004, AJ, 127, 2753
de Marchi, G., Leibundgut, B., Paresce, F., & Pulone, L. 1999, A&A, 343, L9
D'Ercole, A., Vesperini, E., D'Antona, F., McMillan, S. L. W., & Recchi, S. 2008, MNRAS, 391, 825
Dotter, A., Sarajedini, A., & Anderson, J. 2011, ApJ, 738, 74
Frank, M. J., Hilker, M., Baumgardt, H., et al. 2012, MNRAS, 423, 2917
Jordi, K., Grebel, E. K., Hilker, M., et al. 2009, AJ, 137, 4586
Geisler, D., Wallerstein, G., Smith, V. V., & Casetti-Dinescu, D. I. 2007, PASP, 119, 939
Gratton, R. G., Carretta, E., & Bragaglia, A. 2012, A&A Rev., 20, 50
Hanke, M., Koch, A., Hansen, C.J., & McWilliam, A. 2016, A&A, submitted
Harris, W. E. 1996, AJ, 112, 1487
Ishigaki, M. N., Hwang, N., Chiba, M., & Aoki, W. 2016, ApJ, 823, 157
Ivans, I. I., Kraft, R. P., Sneden, C., et al. 2001, AJ, 122, 1438
Johnson, C. I., Rich, R. M., Kobayashi, C., & Fulbright, J. P. 2012, ApJ, 749, 175
Johnson, C. I., Rich, R. M., Kobayashi, C., Kunder, A., & Koch, A. 2014, AJ, 148, 67
Jordi, K., Grebel, E. K., & Ammon, K. 2006, A&A, 460, 339
Jordi, K., & Grebel, E. K. 2010, A&A, 522, A71
Kayser, A., Hilker, M., Grebel, E. K., & Willemsen, P. G. 2008, A&A, 486, 437
Koch, A., & Edvardsson, B. 2002, A&A, 381, 500
Koch, A., Grebel, E. K., Odenkirchen, M., Martínez-Delgado, D., & Caldwell, J. A. R. 2004, AJ, 128, 2274
Koch, A., Côté, P., & McWilliam, A. 2009, A&A, 506, 729
Koch, A., & McWilliam, A. 2010, AJ, 139, 2289
Koch, A., & Côté, P. 2010, A&A, 517, A59
Koch, A., & McWilliam, A. 2014, A&A, 565, A23
Koch, A., McWilliam, A., Preston, G. W., & Thompson, I. B. 2016, A&A, 587, A124
Kuzma, P. B., Da Costa, G. S., Keller, S. C., & Maunder, E. 2015, MNRAS, 446, 3297
Lamb, M. P., Venn, K. A., Shetrone, M. D., Sakari, C. M., & Pritzl, B. J. 2015, MNRAS, 448, 42
Law, D. R., & Majewski, S. R. 2010, ApJ, 718, 1128
Lind, K., Asplund, M., Barklem, P. S., & Belyaev, A. K. 2011, A&A, 528, A103
Marino, A. F., Milone, A. P., Karakas, A. I., et al. 2015, MNRAS, 450, 815
Martell, S. L., & Grebel, E. K. 2010, A&A, 519, A14
McWilliam, A., & Bernstein, R. A. 2008, ApJ, 684, 326-347
Odenkirchen, M., Grebel, E. K., Dehnen, W., Rix, H.-W., & Cudworth, K. M. 2002, AJ, 124, 1497
Odenkirchen, M., Grebel, E. K., Dehnen, W., et al. 2003, AJ, 126, 2385
Odenkirchen, M., Grebel, E. K., Kayser, A., Rix, H.-W., & Dehnen, W. 2009, AJ, 137, 3378
Pearson, S., Küpper, A. H. W., Johnston, K. V., & Price-Whelan, A. M. 2015, ApJ, 799, 28
Ramírez, I., & Meléndez, J. 2005, ApJ, 626, 465
Roederer, I. U., Mateo, M., Bailey, J. I., et al. 2016, MNRAS, 455, 2417
Ruchti, G. R., Feltzing, S., Lind, K., et al. 2016, MNRAS, 461, 2174
Sakari, C. M., Shetrone, M., Venn, K., McWilliam, A., & Dotter, A. 2013, MNRAS, 434, 358
Sandage, A., & Hartwick, F. D. A. 1977, AJ, 82, 459
Sbordone, L., Monaco, L., Moni Bidin, C., et al. 2015, A&A, 579, A104
Schweitzer, A. E., Cudworth, K. M., & Majewski, S. R. 1993, The Globular Cluster-Galaxy Connection, 48, 113
Schönebeck, F., Puzia, T. H., Pasquali, A., et al. 2014, A&A, 572, A13
Smith, G. H. 1985, ApJ, 298, 249
Smith, G. H., Sneden, C., & Kraft, R. P. 2002, AJ, 123, 1502
Tonry, J., & Davis, M. 1979, AJ, 84, 1511
Vogt, S. S., Mateo, M., Olszewski, E. W., & Keane, M. J. 1995, AJ, 109, 151
Walker, M. G., Mateo, M., Olszewski, E. W., Bernstein, R., Sen, B., & Woodroofe, M. 2007, ApJS, 171, 389
Yong, D., Meléndez, J., Cunha, K., et al. 2008, ApJ, 689, 1020-1030